A posteriori local subcell correction of DG schemes through Finite Volume reformulation on unstructured grids

François Vilar

Institut Montpelliérain Alexander Grothendieck, Université de Montpellier

Mai 2021

History

- Introduced by Reed and Hill in 1973 in the frame of the neutron transport
- Major development and improvements by B. Cockburn and C.-W. Shu in a series of seminal papers

Procedure

- Local variational formulation
- Piecewise polynomial approximation of the solution in the cells
- Choice of the numerical fluxes
- Time integration

Advantages

- Natural extension of Finite Volume method
- Excellent analytical properties (L_2 stability, $hp-$adaptivity, ...)
- Extremely high accuracy (superconvergent for scalar conservation laws)
- Compact stencil (involve only face neighboring cells)

Scalar conservation law

- $\partial_t u(\mathbf{x},t) + \nabla_x . \mathbf{F}(u(\mathbf{x},t)) = 0, \qquad (\mathbf{x},t) \in \omega \times [0,T]$
- $u(\mathbf{x},0) = u_0(\mathbf{x}), \qquad \mathbf{x} \in \omega$

$(k+1)^{\text{th}}$ order semi-discretization

- $\{\omega_c\}_c$ a partition of ω, such that $\omega = \bigcup_c \omega_c$
- $u_h(\mathbf{x},t)$ the numerical solution, such that $u_{h|\omega_c} = u_h^c \in \mathbb{P}^k(\omega_c)$

$$u_h^c(\mathbf{x},t) = \sum_{m=1}^{N_k} u_m^c(t)\,\sigma_m(\mathbf{x})$$

- $\{\sigma_m\}_{m=1,\dots,N_k}$ a basis of $\mathbb{P}^k(\omega_c)$, with $N_k = \frac{(k+1)(k+2)}{2}$ in 2D.

Local variational formulation on ω_c

- $\displaystyle\int_{\omega_c} \left(\frac{\partial u}{\partial t} + \nabla_x . \mathbf{F}(u) \right) \psi \,\mathrm{d}V = 0$ with $\psi(\mathbf{x})$ a test function

Integration by parts

- $\int_{\omega_c} \frac{\partial u}{\partial t} \psi \, \mathrm{d}V - \int_{\omega_c} \mathbf{F}(u) \,.\, \nabla_x \psi \, \mathrm{d}V + \int_{\partial \omega_c} \psi \, \mathbf{F}(u) \,.\, \mathbf{n} \, \mathrm{d}S = 0$

Approximated solution

- Substitute u by u_h^c, and restrict ψ to the polynomial space $\mathbb{P}^k(\omega_c)$
- $\int_{\omega_c} \frac{\partial u_h^c}{\partial t} \psi \, \mathrm{d}V = \int_{\omega_c} \mathbf{F}(u_h^c) \,.\, \nabla_x \psi \, \mathrm{d}V - \int_{\partial \omega_c} \psi \, \mathcal{F}_n \, \mathrm{d}S, \qquad \forall \, \psi \in \mathbb{P}^k(\omega_c)$
- $\sum_{m=1}^{N_k} \frac{\mathrm{d}\, u_m^c}{\mathrm{d}t} \int_{\omega_c} \sigma_m \, \sigma_p \, \mathrm{d}V = \int_{\omega_c} \mathbf{F}(u_h^c) \,.\, \nabla_x \sigma_p \, \mathrm{d}V - \int_{\partial \omega_c} \sigma_p \, \mathcal{F}_n \, \mathrm{d}S, \quad \forall \, p \in [\![1, N_k]\!]$

Numerical flux: $\mathcal{F}_n = \mathcal{F}\left(u_h^c, u_h^v, \mathbf{n}\right)$

- $\mathcal{F}(u, v, \mathbf{n}) = \frac{(\mathbf{F}(u) + \mathbf{F}(v))}{2} \,.\, \mathbf{n} - \frac{\gamma(u, v, \mathbf{n})}{2} (v - u)$
- $\gamma(u, v, \mathbf{n}) = \max\left(\left|\mathbf{F}'(u) \,.\, \mathbf{n}\right|, \left|\mathbf{F}'(v) \,.\, \mathbf{n}\right|\right)$ Local Lax-Friedrichs
- $\gamma(u, v, \mathbf{n}) = \sup_w \left(\|\mathbf{F}'(w)\|_2\right)$ Global Lax-Friedrichs

Numerical example: solid body rotation

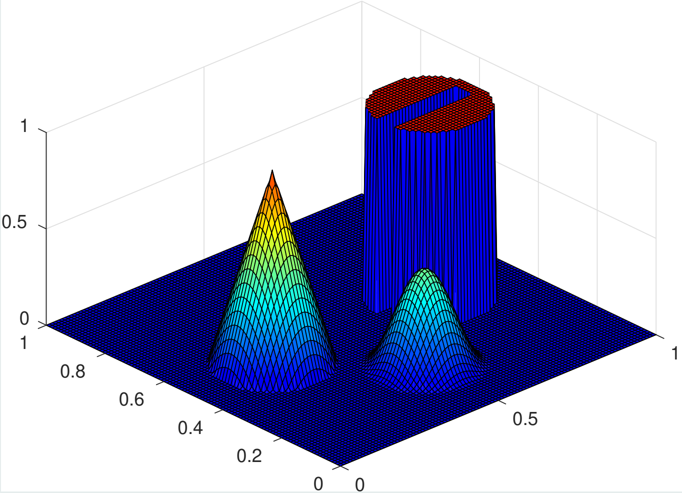

Figure : Rotation of composite signal: initial solution

Roughly constant number of degrees of freedom

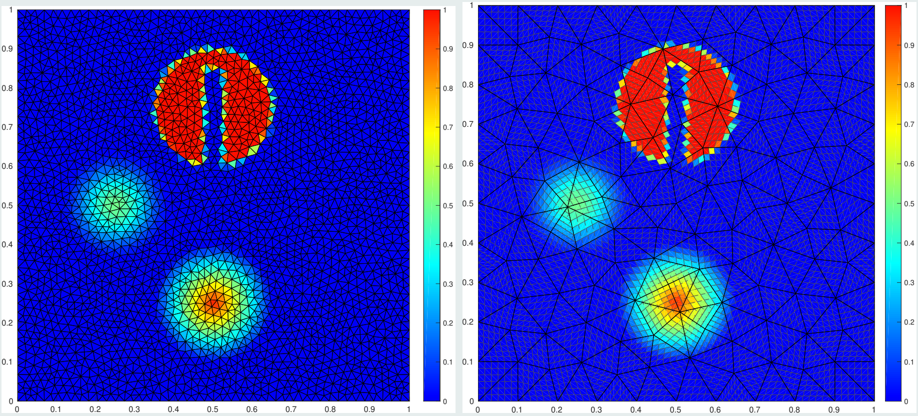

(a) 1st order on 5154 cells

(b) 6th order on 242 cells (5082 DoF)

Figure : Rotation of composite signal: initial solution

Subcell resolution of DG scheme

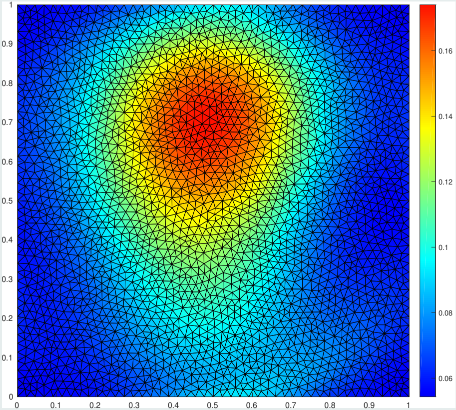

(c) 1st order on 5154 cells

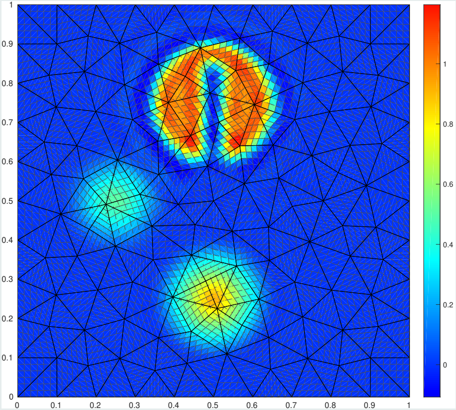

(d) 6th order on 242 cells (5082 DoF)

Figure : Rotation of composite signal after one period: subcells mean value

Subcell resolution of DG scheme

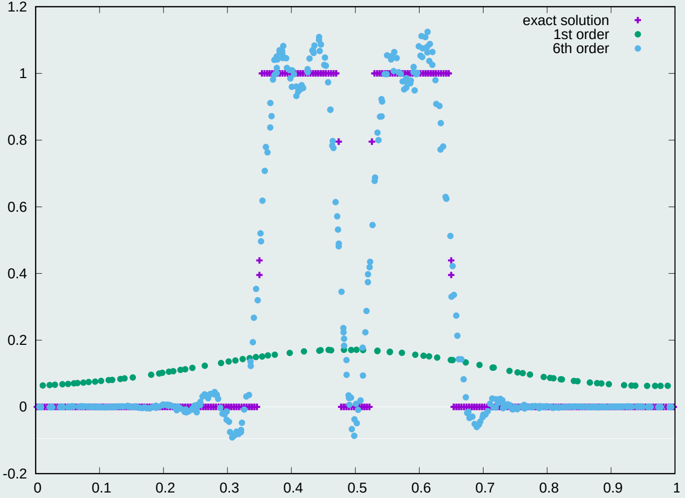

Figure : Rotation of composite signal after one period: profiles for $y = 0.75$

Gibbs phenomenon

- High-order schemes leads to spurious oscillations near discontinuities
- Leads potentially to nonlinear instability, non-admissible solution, crash
- Vast literature of how prevent this phenomenon to happen:

$\Longrightarrow$ *a priori* and ***a posteriori*** limitations

A priori limitation

- Artificial viscosity
- Slope/moment/hierarchical limiter
- ENO/WENO limiter

A posteriori limitation

- MOOD (“Multi-dimensional Optimal Order Detection”)
- Subcell Finite Volume limitation
- **Local subcell correction through flux reconstruction**

F. VILAR, *A Posteriori Correction of High-Order DG Scheme through Subcell Finite Volume Formulation and Flux Reconstruction.* JCP, 2018.

Admissible numerical solution

- Maximum principle / positivity preserving
- Prevent the code from crashing (for instance avoiding NaN)
- **Ensure the conservation of the scheme**

Spurious oscillations

- Discrete maximum principle
- Relaxing condition for smooth extrema

Accuracy

- Retain as much as possible the subcell resolution of the DG scheme
- Minimize the number of subcell solutions to recompute

Modify locally, at the subcell level, the numerical solution without impacting the solution elsewhere in the cell

DG as a subcell Finite Volume

- Rewrite DG scheme as a specific Finite Volume scheme on subcells
- Exhibit the corresponding subcell numerical fluxes: **reconstructed flux**

Cell subdivision into N_k subcells

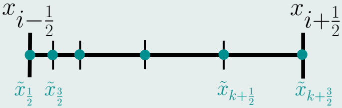

Figure : Example of a subdivision for a $\mathbb{P}^k$ DG scheme in 1D

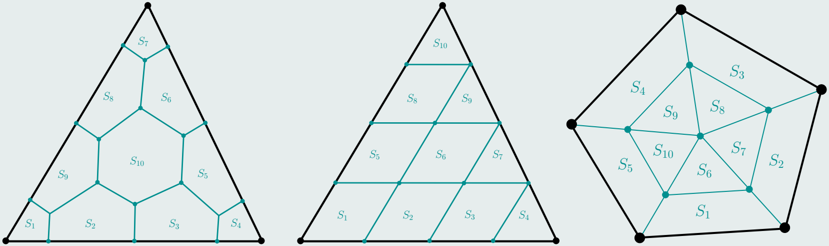

Figure : Examples of subdivision for a $\mathbb{P}^3$ DG scheme in 2D

DG schemes through residuals

- $$\sum_{m=1}^{N_k} \frac{\mathrm{d}\, u_m^c}{\mathrm{d}t} \int_{\omega_c} \sigma_m \, \sigma_p \, \mathrm{d}V = \int_{\omega_c} \mathbf{F}(u_h^c) \, . \, \nabla_x \sigma_p \, \mathrm{d}V - \int_{\partial \omega_c} \sigma_p \, \mathcal{F}_n \, \mathrm{d}S, \quad \forall \, p \in [\![1, N_k]\!]$$

$$\Longrightarrow \quad \boxed{M_c \, \frac{\mathrm{d}\, U_c}{\mathrm{d}t} = \Phi_c}$$

- $(U_c)_m = u_m^c$ — Solution moments
- $(M_c)_{mp} = \int_{\omega_c} \sigma_m \, \sigma_p \, \mathrm{d}V$ — Mass matrix
- $(\Phi_c)_m = \int_{\omega_c} \mathbf{F}(u_h^c) \, . \, \nabla_x \sigma_m \, \mathrm{d}V - \int_{\partial \omega_c} \sigma_m \, \mathcal{F}_n \, \mathrm{d}S$ — DG residuals

Subdivision and definition

- ω_c is subdivided into N_k subcells S_m^c
- Let us define $\overline{\psi}_m^c = \frac{1}{|S_m^c|} \int_{S_m^c} \psi \, \mathrm{d}V$ the subcell mean value

Submean values

- $$\int_{S_m^c} \frac{\partial u_h^c}{\partial t}\, \mathrm{d}V = |S_m^c| \frac{\mathrm{d}\, \overline{u}_m^c}{\mathrm{d}t}$$
- $$\frac{\mathrm{d}\, \overline{u}_m^c}{\mathrm{d}t} = \frac{1}{|S_m^c|} \sum_{q=1}^{N_k} \frac{\mathrm{d}\, u_q^c}{\mathrm{d}t} \int_{S_m^c} \sigma_q \, \mathrm{d}V$$

$$\Longrightarrow \quad \boxed{\frac{\mathrm{d}\, \overline{U}_c}{\mathrm{d}t} = P_c \frac{\mathrm{d}\, U_c}{\mathrm{d}t}}$$

- $(\overline{U}_c)_m = \overline{u}_m^c$ — Submean values
- $(P_c)_{mp} = \dfrac{1}{|S_m^c|} \displaystyle\int_{S_m^c} \sigma_p \, \mathrm{d}V$ — Projection matrix

$$\Longrightarrow \quad \boxed{\frac{\mathrm{d}\, \overline{U}_c}{\mathrm{d}t} = P_c \, M_c^{-1} \, \Phi_c}$$

Subcell Finite Volume: reconstructed fluxes

- Let us introduce the reconstructed fluxes such that

$$\boxed{\frac{\mathrm{d}\,\overline{u}_m^c}{\mathrm{d}t} = -\frac{1}{|S_m^c|}\int_{\partial S_m^c} \widehat{F_n}\,\mathrm{d}S}$$

- We impose that on the boundary of cell ω_c

$$\boxed{\widehat{F_n}_{|\partial\omega_c} = \mathcal{F}_n}$$

- $\displaystyle \frac{\mathrm{d}\,\overline{u}_m^c}{\mathrm{d}t} = -\frac{1}{|S_m^c|}\left(\sum_{f_{qq'}\in f_m^c}\int_{f_{qq'}} \widehat{F_n}\,\mathrm{d}S + \int_{\partial S_m^c\cap\partial\omega_c} \mathcal{F}_n\,\mathrm{d}S\right)$
- f_m^c Set of faces in $\partial S_m^c \setminus \partial\omega_c$
- $\displaystyle \int_{f_{qq'}} \widehat{F_n}\,\mathrm{d}S = \varepsilon_{qq'}\,\widehat{F_{qq'}}$
- $\varepsilon_{qq'}$ Sign function depending on the orientation of face $f_{qq'}$

Subcell Finite Volume: reconstructed fluxes

- $$\varepsilon_{qq'} = \begin{cases} 1 & \text{if the face } f_{qq'} \text{ is direct} \\ -1 & \text{if the edge } f_{qq'} \text{ is indirect} \\ 0 & \text{if } f_{qq'} \notin f_c = \bigcup_{m=1}^{N_k} f_m^c \end{cases}$$
- Let $\widehat{F_c}$ be the vector containing all the interior faces reconstructed fluxes
- The subcell mean values governing equations yield the following system

$$\boxed{-A_c\,\widehat{F_c} = D_c\,\frac{\mathrm{d}\,\overline{U}_c}{\mathrm{d}t} + B_c}$$

- $(A_c)_{qq'} = \varepsilon_{qq'}$ Adjacency matrix
- $D_c = \mathrm{diag}\left(|S_1^c|, \ldots, |S_{N_k}^c|\right)$ Subcells volume matrix
- $(B_c)_m = \int_{\partial S_m^c \cap \partial \omega_c} \mathcal{F}_n \,\mathrm{d}S$ Cell boundary contribution

Subcell Finite Volume: reconstructed fluxes

- Introducing $Q_c = D_c\, P_c$ such that $(Q_c)_{mp} = \displaystyle\int_{S_m^c} \sigma_p \,\mathrm{d}V$, one finally gets

$$\boxed{-A_c\,\widehat{F_c} = Q_c\, M_c^{-1}\, \Phi_c + B_c}$$

Graph Laplacian technique

- $A_c \in \mathcal{M}_{N_k \times N_F}$ with $N_F = \mathrm{Card}(\mathcal{S}_c)$ the number of interior faces
- $A_c^{\mathrm{t}}\, \mathbf{1} = \mathbf{0}$ where $\mathbf{1} = (1, \dots, 1)^{\mathrm{t}} \in \mathbb{R}^{N_k}$

R. Abgrall, *Some Remarks about Conservation for Residual Distribution Schemes.* Methods Appl. Math., 18:327-351, 2018.

- Let $\mathcal{L}_c^{-1}$ be the inverse of $L_c = A_c\, A_c^{\mathrm{t}}$ on the orthogonal of its kernel

$$\boxed{\mathcal{L}_c^{-1} = (L_c + \lambda\,\Pi)^{-1} - \frac{1}{\lambda}\,\Pi} \qquad \forall \lambda \neq 0$$

- $\Pi = \frac{1}{N_k}\,(\mathbf{1} \otimes \mathbf{1}) \in \mathcal{M}_{N_k}$

Graph Laplacian technique

- Finally, we obtain the following definition of the reconstructured fluxes

$$\boxed{\widehat{F_c} = -A_c^{\mathrm{t}}\,\mathcal{L}_c^{-1}\left(Q_c\,M_c^{-1}\,\Phi_c + B_c\right)}$$

remark

- The only terms depending on the time are Φ_c and B_c

Back to the DG scheme

- The polynomial solution is defined through reconstructed fluxes as follows

$$\boxed{\frac{\mathrm{d}\,U_c}{\mathrm{d}t} = -Q_c^{-1}\left(A_c\,\widehat{F_c} + B_c\right)}$$

Question

- Is the reconstructed flux $\widehat{F_c}$ close to the interior flux $\boldsymbol{F}(u_h^c)$?

Local variational formulation

- $$\int_{\omega_c} \frac{\partial u_h^c}{\partial t}\,\psi\,\mathrm{d}V = \int_{\omega_c} \mathbf{F}(u_h^c)\,.\,\nabla_x\psi\,\mathrm{d}V - \int_{\partial\omega_c}\psi\,\mathcal{F}_n\,\mathrm{d}S, \qquad \forall\,\psi\in\mathbb{P}^k(\omega_c)$$
- Substitute $\boldsymbol{F}(u_h^c)$ with $\boldsymbol{F}_h^c \in \left(\mathbb{P}^{k+1}(\omega_c)\right)^2$ (collocated or L_2 projection)
- $$\int_{\omega_c} \frac{\partial u_h^c}{\partial t}\,\psi\,\mathrm{d}V = -\int_{\omega_c}\psi\,\nabla_x\,.\,\boldsymbol{F}_h^c\,\mathrm{d}V + \int_{\partial\omega_c}\psi\left(\boldsymbol{F}_h^c\,.\,\boldsymbol{n} - \mathcal{F}_n\right)\mathrm{d}S, \quad \forall\,\psi\in\mathbb{P}^k(\omega_c)$$

Subresolution basis functions

- Let us introduce the N_k basis functions $\{\phi_m\}_m$ such that $\forall\,\psi\in\mathbb{P}^k(\omega_c)$

$$\int_{\omega_c}\phi_m\,\psi\,\mathrm{d}V = \int_{S_m^c}\psi\,\mathrm{d}V, \qquad \forall\,m=1,\dots,N_k,$$

- $$\sum_{m=1}^{N_k}\phi_m(\boldsymbol{x}) = 1$$

These particular functions can be seen as the L_2 projection of the indicator functions $\mathbb{1}_m(\boldsymbol{x})$ onto $\mathbb{P}^k(\omega_c)$

Subcell Finite Volume scheme

- $\displaystyle\int_{\omega_c} \frac{\partial u_h^c}{\partial t}\, \phi_m \,\mathrm{d}V = -\int_{\omega_c} \phi_m \,\nabla_x \cdot \boldsymbol{F}_h^c \,\mathrm{d}V + \int_{\partial\omega_c} \phi_m \,\left(\boldsymbol{F}_h^c \cdot \boldsymbol{n} - \mathcal{F}_n\right) \mathrm{d}S$
- $\displaystyle|S_m^c| \frac{\mathrm{d}\,\overline{u}_m^c}{\mathrm{d}t} = -\int_{S_m^c} \nabla_x \cdot \boldsymbol{F}_h^c \,\mathrm{d}V + \int_{\partial\omega_c} \phi_m \,\left(\boldsymbol{F}_h^c \cdot \boldsymbol{n} - \mathcal{F}_n\right) \mathrm{d}S$
- $\displaystyle\frac{\mathrm{d}\,\overline{u}_m^c}{\mathrm{d}t} = -\frac{1}{|S_m^c|}\left(\int_{\partial S_m^c} \boldsymbol{F}_h^c \cdot \boldsymbol{n} \,\mathrm{d}S - \int_{\partial\omega_c} \phi_m \,\left(\boldsymbol{F}_h^c \cdot \boldsymbol{n} - \mathcal{F}_n\right) \mathrm{d}S\right)$
- $\displaystyle\frac{\mathrm{d}\,\overline{u}_m^c}{\mathrm{d}t} = -\frac{1}{|S_m^c|} \int_{\partial S_m^c} \widehat{F_n} \,\mathrm{d}S$ Subcell Finite Volume

Reconstructed Fluxes

- Finally, we get that

$$\boxed{\int_{\partial S_m^c} \widehat{F_n} \,\mathrm{d}S = \int_{\partial S_m^c} \boldsymbol{F}_h^c \cdot \boldsymbol{n} \,\mathrm{d}S - \int_{\partial\omega_c} \phi_m \,\left(\boldsymbol{F}_h^c \cdot \boldsymbol{n} - \mathcal{F}_n\right) \mathrm{d}S}$$

Reconstructed fluxes

- As we impose that $\widehat{F_n}_{|\partial\omega_c} = \mathcal{F}_n$, this last expression rewrites

$$\int_{\partial S_m^c \setminus \partial\omega_c} \widehat{F_n}\, \mathrm{d}S = \int_{\partial S_m^c \setminus \partial\omega_c} \boldsymbol{F}_h^c \,\boldsymbol{.}\, \boldsymbol{n} \,\mathrm{d}S - \int_{\partial\omega_c} \widetilde{\phi_m} \left(\boldsymbol{F}_h^c \,\boldsymbol{.}\, \boldsymbol{n} - \mathcal{F}_n\right) \mathrm{d}S$$

- $\widetilde{\phi_m} = \begin{cases} \phi_m & \text{if } \boldsymbol{x} \in \partial\omega_c \setminus \partial S_m^c \\ \phi_m - 1 & \text{if } \boldsymbol{x} \in \partial\omega_c \bigcap \partial S_m^c \end{cases}$

- $\displaystyle\int_{f_{qq'}} \widehat{F_n}\, \mathrm{d}S = \varepsilon_{qq'}\, \widehat{F_{qq'}}$ and $\displaystyle\int_{f_{qq'}} \boldsymbol{F}_h^c \,\boldsymbol{.}\, \boldsymbol{n} \,\mathrm{d}S = \varepsilon_{qq'}\, F_{qq'}$

- Then, if F_c is the vector containing all the interior faces fluxes, one gets

$$\boxed{A_c\, \widehat{F_c} = A_c\, F_c - G_c}$$

- $(G_c)_m = \displaystyle\int_{\partial\omega_c} \widetilde{\phi_m} \left(\boldsymbol{F}_h^c \,\boldsymbol{.}\, \boldsymbol{n} - \mathcal{F}_n\right) \mathrm{d}S$ Boundary contribution

Reconstructed fluxes through interior fluxes

- Making use of the same graph Laplacian technique, we finally obtain

$$\boxed{\widehat{F_c} = F_c - A_c^{t}\,\mathcal{L}_c^{-1}\,G_c}$$

- We can rewrite this expression as

$$\widehat{F_c} = F_c - E\big(\boldsymbol{F}_h^c \boldsymbol{.}\, \boldsymbol{n} - \mathcal{F}_n\big)$$

where $E(.)$ is a correction function taking into account the jump between the polynomial flux and the numerical flux on the cell boundary

Remark

- Different choice in the correction term $E(.)$ leads to different schemes
- For instance, $E(.) = 0$ leads to the spectral volume scheme of Z.J. Wang

Reconstructed flux in the 1D case

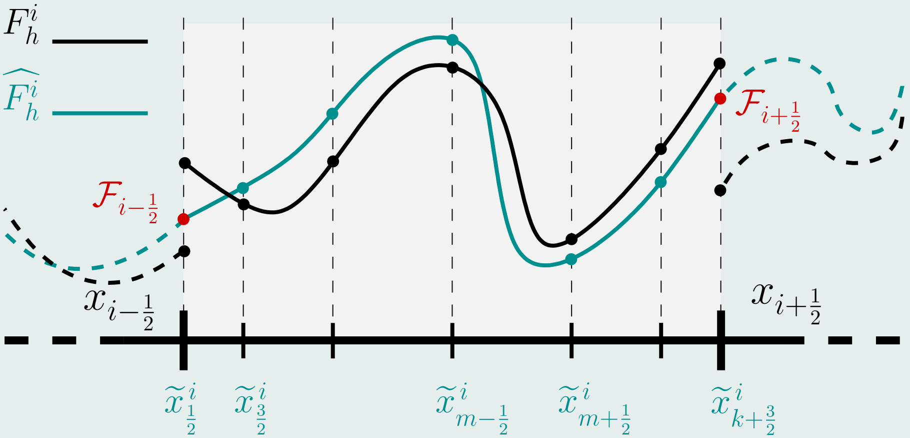

Figure : Polynomial interior flux and reconstructed flux

RKDG scheme

- SSP Runge-Kutta: convex combinations of first-order forward Euler
- For sake of clarity, we focus on forward Euler time stepping

Projection on subcells of RKDG solution

- $u_h^{c,n}(x) = \sum_{m=1}^{N_k} u_m^{c,n}\, \sigma_m(x)$
- $u_h^{c,n}$ is uiquely defined by its N_k submean values $\overline{u}_m^{c,n}$
- Recalling the definition of the projection matrix $(P_c)_{mp} = \dfrac{1}{|S_m^c|} \displaystyle\int_{S_m^c} \sigma_p \,\mathrm{d}V,$

$$\Longrightarrow \qquad P_c \begin{pmatrix} u_1^{c,n} \\ \vdots \\ u_{N_k}^{c,n} \end{pmatrix} = \begin{pmatrix} \overline{u}_1^{c,n} \\ \vdots \\ \overline{u}_{N_k}^{c,n} \end{pmatrix}$$

Set up

- We assume that, for each cell, the $\{\overline{u}_m^{c,n}\}_m$ are admissible
- Compute a candidate solution u_h^{n+1} from u_h^n through uncorrected DG
- For each subcell, check if the submean values $\{\overline{u}_m^{c,n+1}\}_m$ are ok

Physical admissibility detection (PAD)

- Check if $\overline{u}_m^{c,n+1}$ lies in an convex physical admissible set (maximum principle for SCL, positivity of the pressure and density for Euler, ...)
- Check if there is any *NaN* values

Numerical admissibility detection (NAD)

- Discrete maximum principle DMP on submean values:

$$\min_{v\in\mathcal{V}(S_m^c)} \left(\overline{u}_v^n\right) \leq \overline{u}_m^{c,n+1} \leq \max_{v\in\mathcal{V}(S_m^c)} \left(\overline{u}_v^n\right)$$

- $\mathcal{V}(S_m^c)$ set of neighboring subcells of S_m^c, including subcell S_m^c
- **This criterion needs to be relaxed to preserve smooth extrema**

Fundamental principle

- On non-admissible subcell boundaries

Substitute the reconstructed fluxes by more robust numerical fluxes

- Recompute the non-admissible subcells, and their first neighbors

Examples of correction schemes

- **1st-order Finite Volume scheme**
- 2nd-order MUSCL scheme
- (W)ENO methods
- . . .

Corrected reconstructed flux

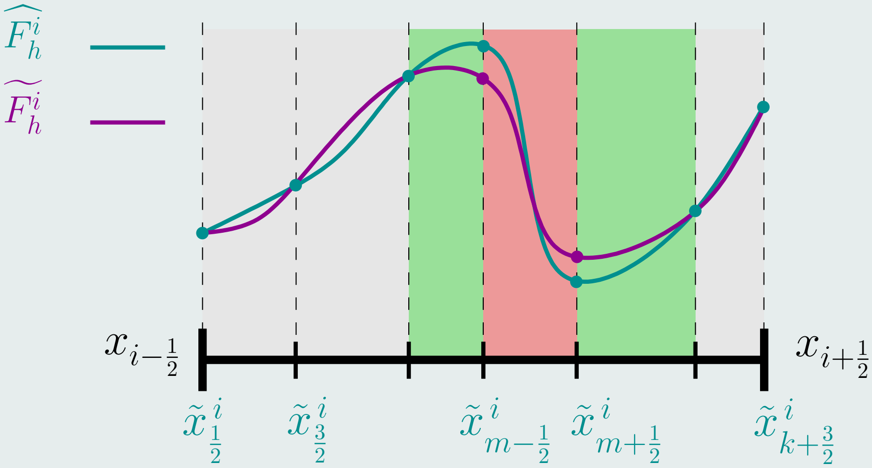

Figure : Correction of the reconstructed flux

Corrected reconstructed flux

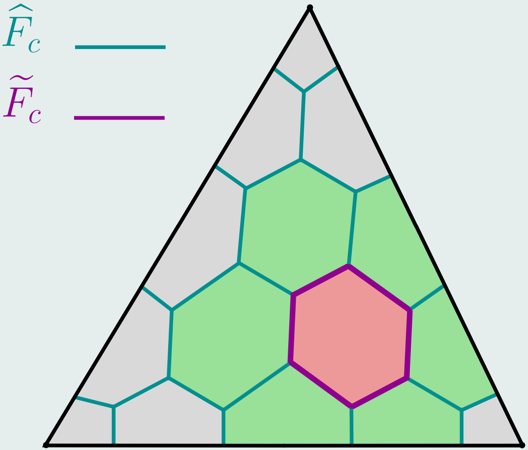

Figure : Correction of the reconstructed flux

Flowchart

1. Compute the uncorrected DG candidate solution $u_h^{c,n+1}$
2. Project $u_h^{c,n+1}$ to get the submean values $\overline{u}_m^{c,n+1}$
3. Check $\overline{u}_m^{c,n+1}$ through the troubled zone detection plus relaxation
4. If $\overline{u}_m^{c,n+1}$ is admissible go further in time, otherwise modify the corresponding reconstructed flux values

$$\forall\, f_{mq} \in \partial S_m^c, \qquad \boxed{\widetilde{F_{mq}} = \mathcal{F}\left(\overline{u}_m^{c,n}, \overline{u}_q^{c,n}, \boldsymbol{n}_{mq}\right)}$$

5. Through the corrected reconstructed flux, recompute the submean values for tagged subcells and their first neighbors
6. Return to 3

Conclusion

- The limitation only affects the DG solution at the subcell scale
- The corrected scheme is conservative at the subcell level
- In practice, few submean values need to be recomputed

Remarks

- For non-linear problems, using very high-order schemes and coarse meshes, the solution may remain a bit oscillatory at the subcell level
- This is why we were previously considering, for $k \geq 3$, that if a subcell is marked as bad then we also mark its first neighboring subcells

F. VILAR, *A Posteriori Correction of High-Order DG Scheme through Subcell Finite Volume Formulation and Flux Reconstruction.* JCP, 2018.

New correction principle

To avoid too much discrepancy between corrected and reconstructed fluxes

- Wider subcell set to be corrected
- Convex combination between 1st-order flux and the reconstructed flux

$$\boxed{\widetilde{F_{mq}} = (1 - \theta_{mq})\, \mathcal{F}\left(\overline{u}_m^{c,n}, \overline{u}_q^{c,n}, \boldsymbol{n}_{mq}\right) + \theta_{mq}\, \widehat{F_{mq}},}$$

where θ_{mq} is a function of the distance to the non-admissible subcell

Burgers equation with $u_0(x, y) = \sin(2\pi\,(x + y))$

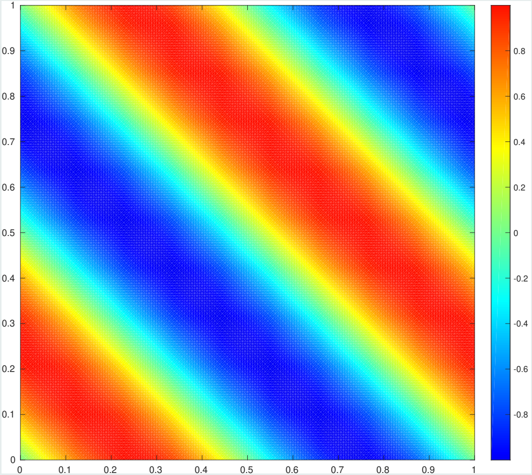

Figure : Entropic weak solution: apparition of stationary shocks

6th-order scheme on a 576 cells grid

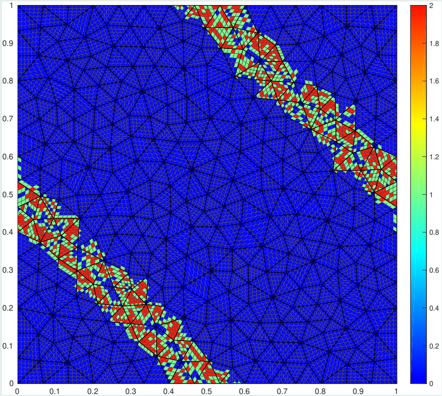

(a) Original correction

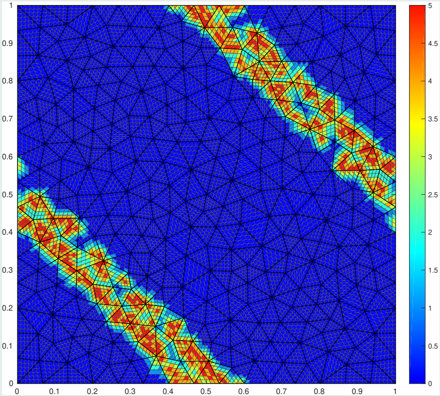

(b) New correction

Figure : Comparison between original and new correction procedure: corrected subcells

6th-order scheme on a 576 cells grid

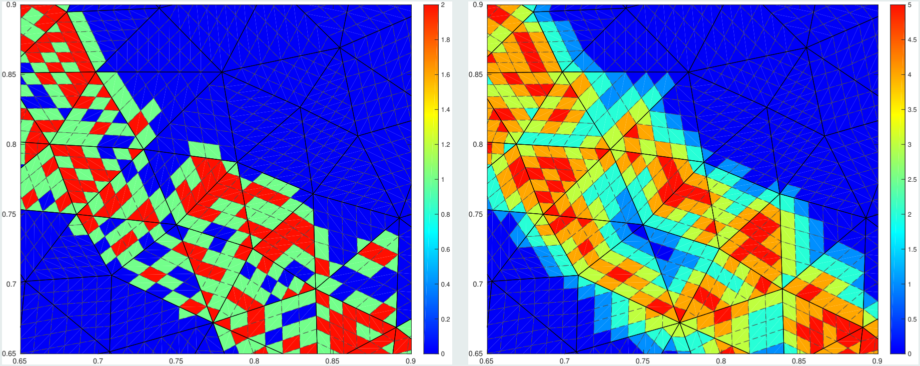

(a) Original correction (b) New correction

Figure : Comparison between original and new correction procedure: corrected subcells

6th-order scheme on a 576 cells grid

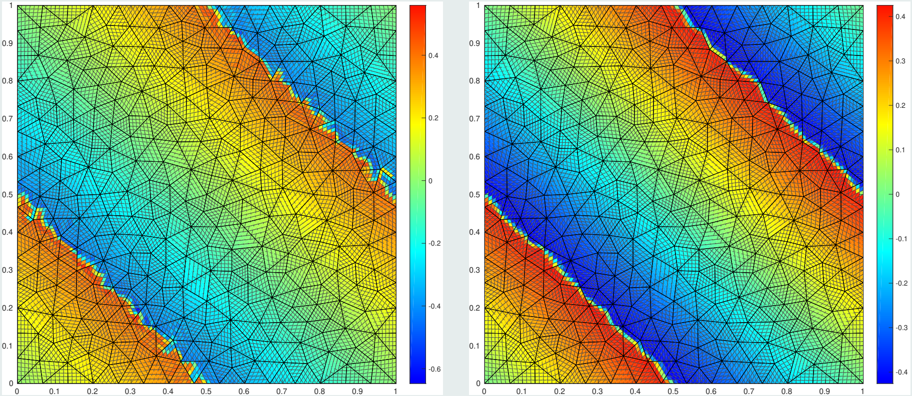

(a) Original correction

(b) New correction

Figure : Comparison between original and new correction procedure: solutions

6th-order scheme on a 576 cells grid

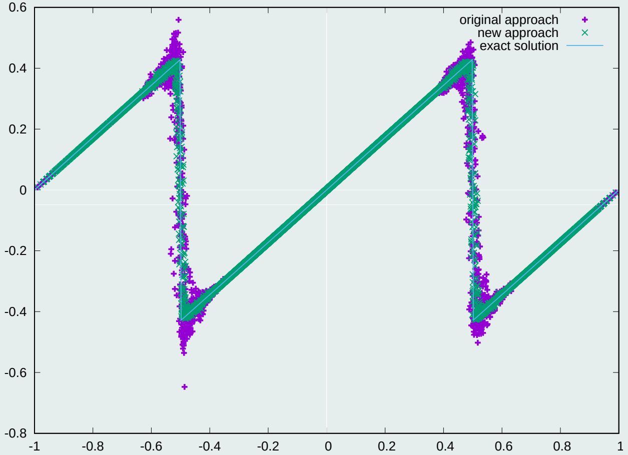

Figure : Comparison between original and new correction procedure: solutions profiles

1D Linear advection

- $\partial_t u(x,t) + c\,\partial_x u(x,t) = 0$ with c transport velocity
- $u(x,0) = u_0(x)$

Linear advection of a square signal after 1 period

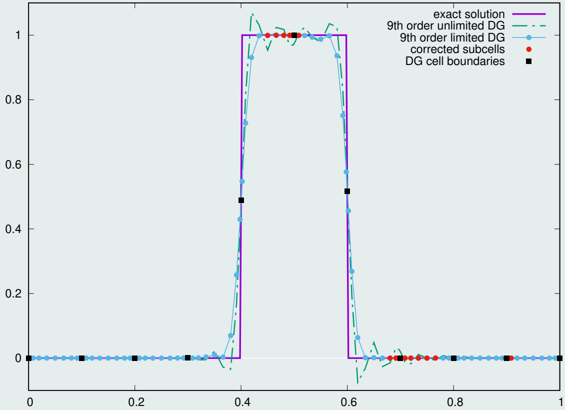

Figure : 9th-order corrected and uncorrected DG solutions with 10 cells

Linear advection of a composite signal after 4 periods

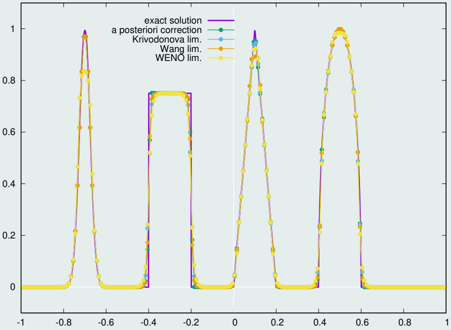

(a) 200 cells: cell mean values

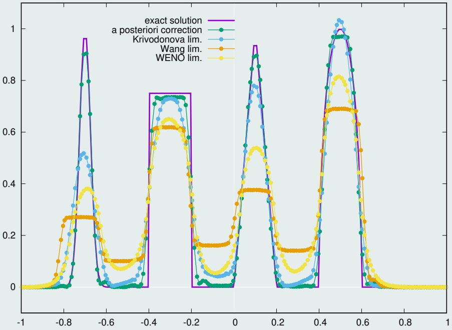

(b) 50 cells: subcell mean values

Figure : 4th-order DG solutions provided different limitations

Linear advection of a composite signal after 4 periods

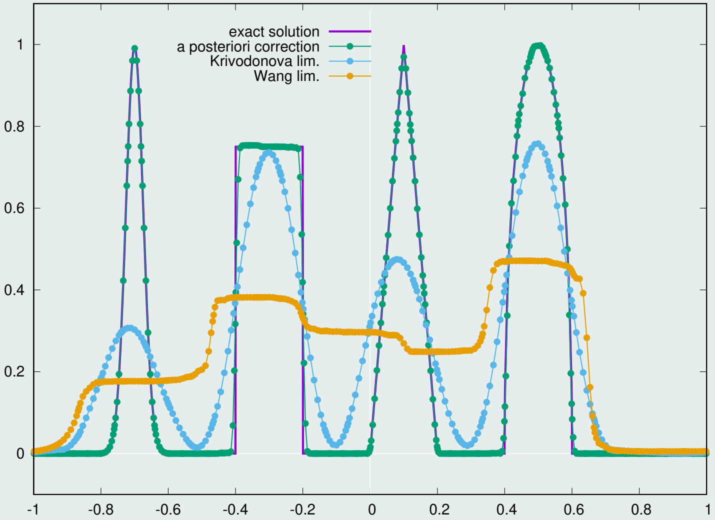

Figure : 9th-order DG solutions provided different limitations with 30 cells

Buckley non-linear non-convex flux problem

- $\partial_t u(x,t) + \partial_x F(u(x,t)) = 0$ with $F(u) = \dfrac{4u^2}{4u^2 + (1-u)^2}$
- $u(x,0) = u_0(x)$

Buckley problem at time $t = 0.4$ **quadrature issue**

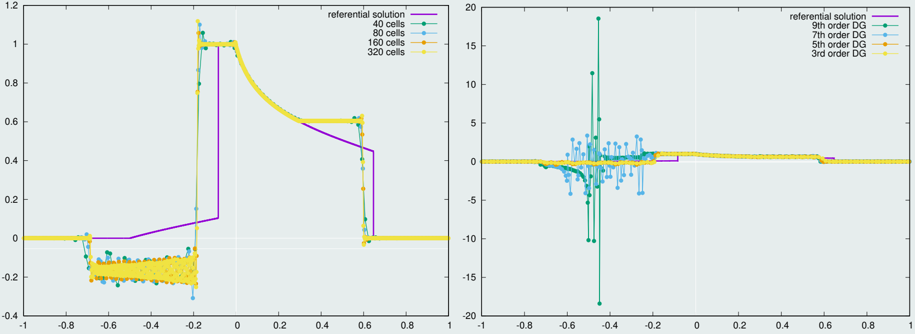

(a) Non-entropic behavior (b) Aliasing phenomenon

Figure : Uncorrected DG solution for the Buckley non-convex flux case

Buckley non-convex flux problem at time $t = 0.4$

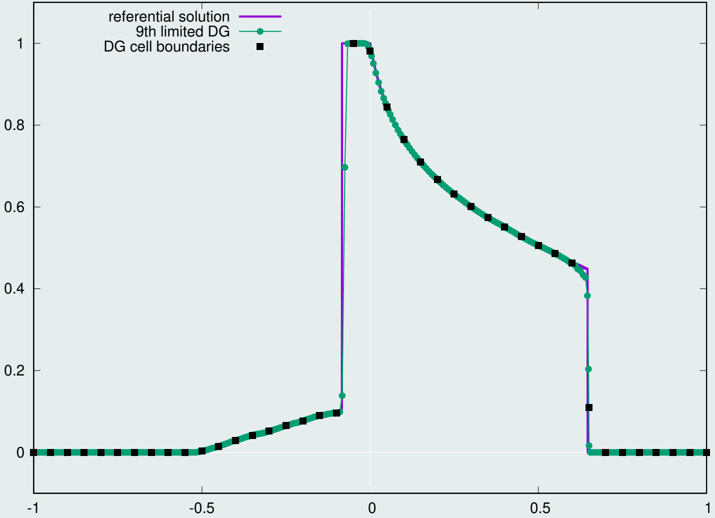

Figure : 9th-order corrected DG solutions on 40 cells

Buckley non-convex flux problem at time $t = 0.4$

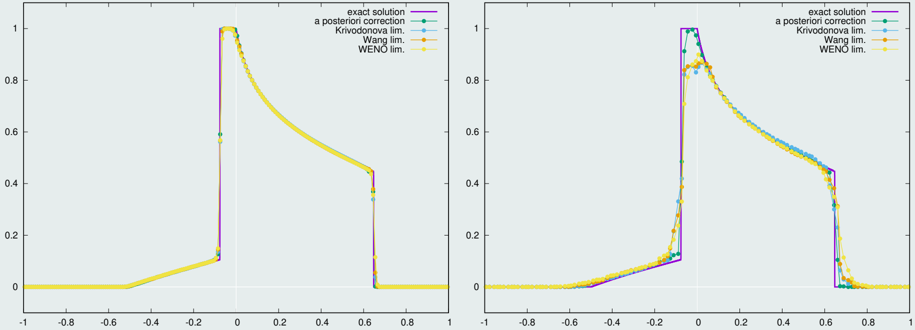

(a) 200 cells: cell mean values

(b) 30 cells: subcell mean values

Figure : 4th-order DG solutions provided different limitations

Buckley non-convex flux problem at time $t = 0.4$

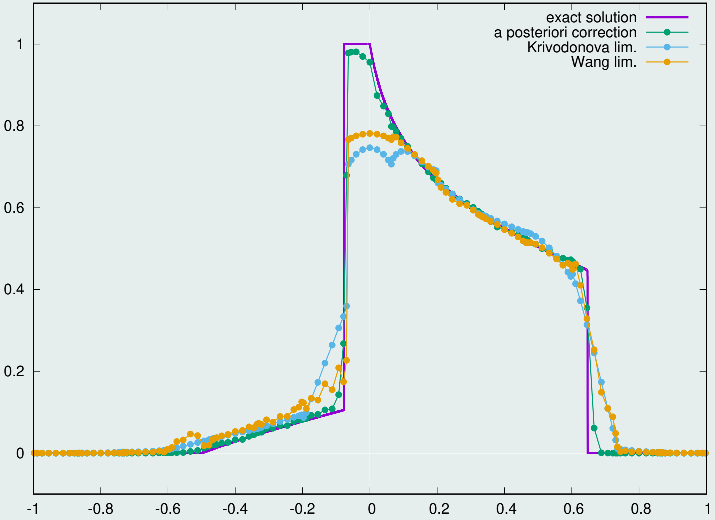

Figure : 9th-order DG solutions provided different limitations on 15 cells

1D non-linear shallow water equations - prebalanced formulation

- $\partial_t \boldsymbol{V} + \partial_x \boldsymbol{F}(\boldsymbol{V}, b) = \boldsymbol{B}(\boldsymbol{V}, \partial_x b)$

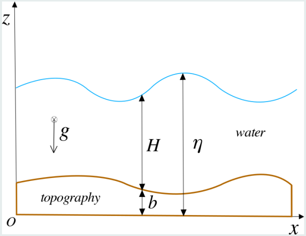

- $\boldsymbol{V} = \begin{pmatrix} \eta \\ q \end{pmatrix}$ conservative variables

- $\boldsymbol{F}(\boldsymbol{V}, b) = \begin{pmatrix} q \\ \frac{q^2}{\eta - b} + g\,(\frac{\eta^2}{2} - 2\,\eta\,b) \end{pmatrix}$ flux function

- $\boldsymbol{B}(\boldsymbol{V}, \partial_x b) = \begin{pmatrix} 0 \\ -g\,\eta\,\partial_x b \end{pmatrix}$ source term

Carrier and Greenspan's periodic solution on a plane beach

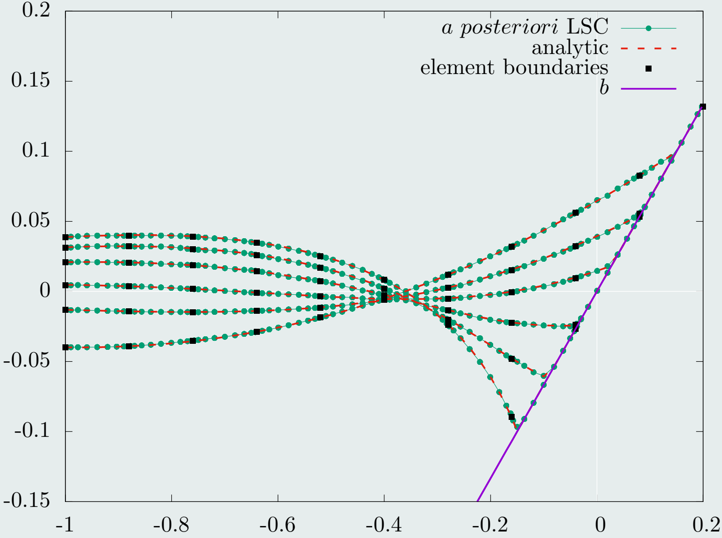

Figure : 9th-order numerical solution with 10 cells: free surface elevation

Synolakis solitary wave on a plane beach

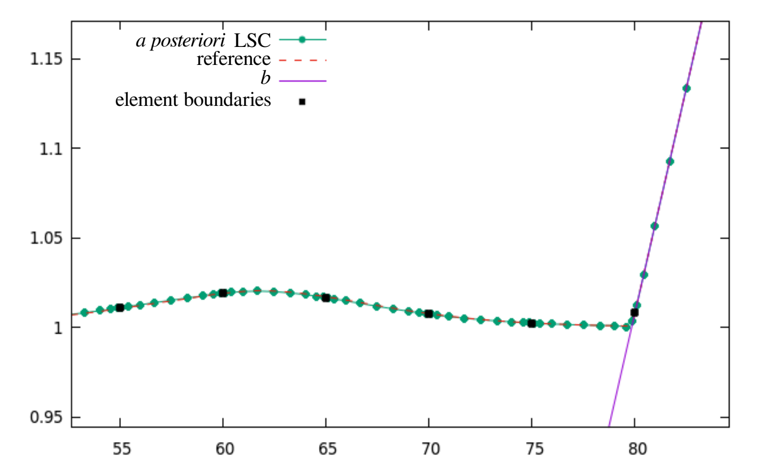

Figure : 9th-order numerical solution with 20 cells: free surface elevation

1D non-linear Euler compressible gas dynamics equations

- $\partial_t \boldsymbol{V} + \partial_x \boldsymbol{F}(\boldsymbol{V}) = \boldsymbol{0}$

- $\boldsymbol{V} = \begin{pmatrix} \rho \\ q \\ E \end{pmatrix}$ <u>conservative variables</u>

- $\boldsymbol{F}(\boldsymbol{V}) = \begin{pmatrix} q \\ \dfrac{q^2}{\rho} + p \\ (E+p)\,\dfrac{q}{\rho} \end{pmatrix}$ <u>flux function</u>

- $p := p(\boldsymbol{V}) = (\gamma - 1)\left(E - \dfrac{q^2}{2\,\rho}\right)$ <u>equation of state</u>

Initial solution on $x \in [0,1]$ for $\gamma = 3$

- $\rho_0(x) = 1 + 0.9999999\sin(\pi x), \quad u_0(x) = 0, \quad p_0(x) = (\rho_0(x))^\gamma$
  $$\Longrightarrow \rho_0(-\tfrac{1}{2}) = 1.E-7 \quad \text{and} \quad p_0(-\tfrac{1}{2}) = 1.E-21$$
- Periodic boundary conditions

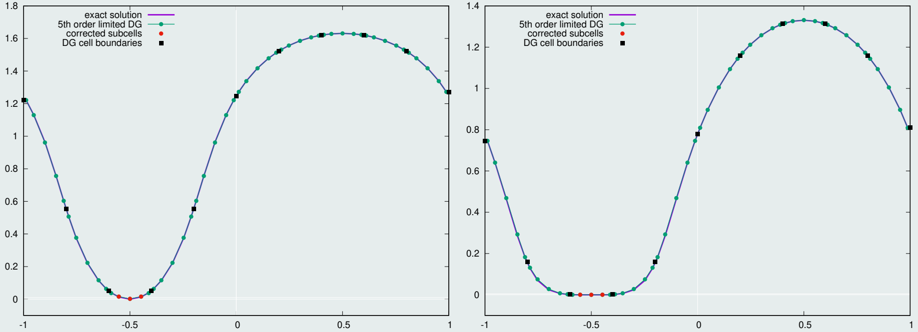

(a) Density (b) Internal energy

Figure : 5th-order corrected DG solution on 10 cells at $t = 0.1$

Convergence rates

	L_1		L_2		Average % of corrected subcells
h	$E^h_{L_1}$	$q^h_{L_1}$	$E^h_{L_2}$	$q^h_{L_2}$	
$\frac{1}{20}$	1.48E-5	4.35	2.02E-5	4.18	6.87 %
$\frac{1}{40}$	9.09E-7	4.88	1.38E-6	4.87	3.31 %
$\frac{1}{80}$	3.09E-8	4.95	4.73E-8	4.86	2.50 %
$\frac{1}{160}$	1.00E-9	-	1.63E-9	-	1.12 %

Table: Convergence rates on the pressure for the Euler equation for a 5th-order DG

Sod shock tube problem

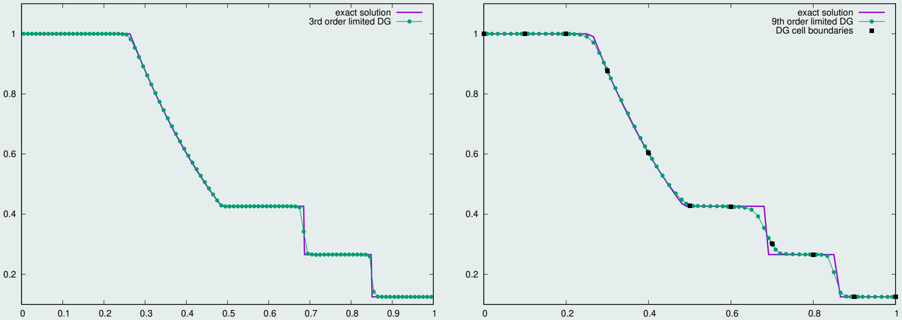

(a) 3rd-order and 100 cells: cell values

(b) 9th-order and 10 cells: subcell values

Figure : Numerical solutions density for Sod shock tube problem

NAD: neighboring subcells set **linear problems**

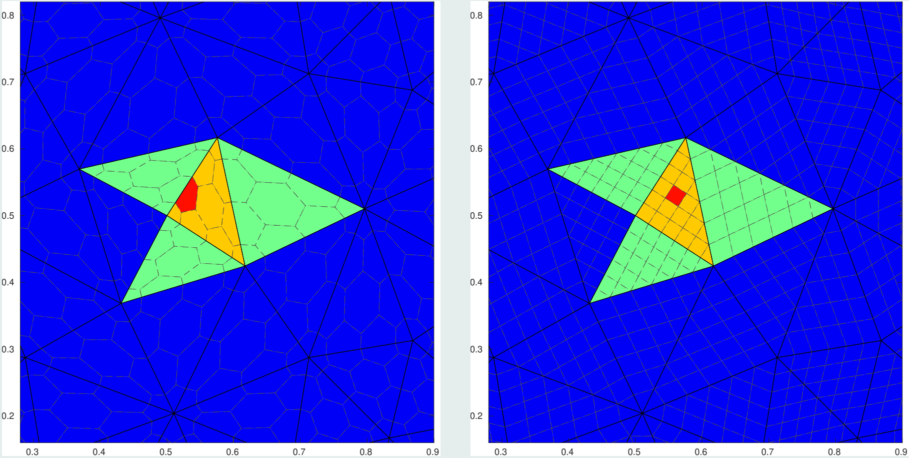

(a) 4th-order, polygonal subdivision

(b) 6th-order, structured subdivision

Figure : Neighboring subcells set for the numerical admissibility criterion

2D Linear advection

- $\partial_t u(\boldsymbol{x},t) + \boldsymbol{A} \boldsymbol{.} \nabla_x u(\boldsymbol{x},t) = 0$ with $\boldsymbol{A}$ transport velocity
- $u(\boldsymbol{x},0) = u_0(\boldsymbol{x})$

Linear advection with $u_0(x,y) = \sin(2\pi\,(x+y))$ and $\boldsymbol{A} = (1,\,1)^t$

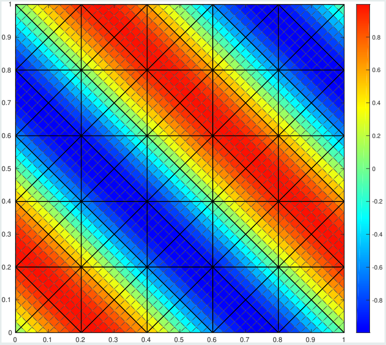

(a) Solution map

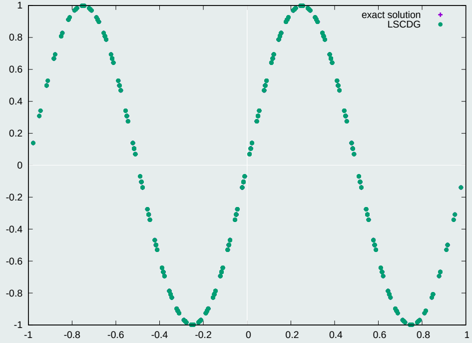

(b) Solution profile

Figure : Linear advection with a 6th DG scheme and 5x5x4 grid after 1 period

Convergence rates

	L_1		L_2		L_∞	
h	$E^h_{L_1}$	$q^h_{L_1}$	$E^h_{L_2}$	$q^h_{L_2}$	$E^h_{L_\infty}$	$q^h_{L_\infty}$
$\frac{1}{10}$	1.62E-5	6.00	1.81E-5	6.00	3.98E-5	5.96
$\frac{1}{20}$	2.53E-7	6.00	2.82E-7	6.00	6.38E-7	5.98
$\frac{1}{40}$	3.95E-9	-	4.41E-9	-	1.01E-8	-

Table: Convergence rates for the linear advection case for a 6th-order DG scheme

Linear advection equation of a crenel signal $\boldsymbol{A} = (1,\ 1)^t$

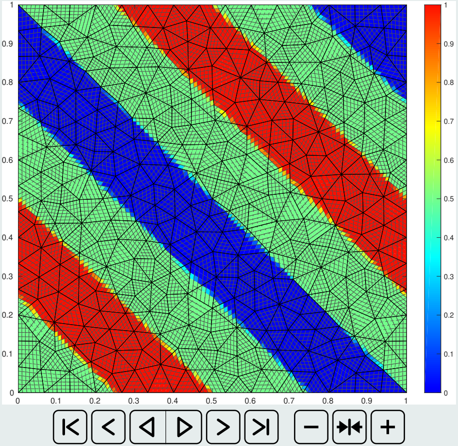

(a) Solution map

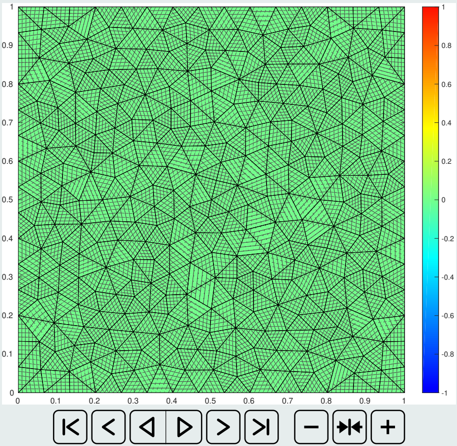

(b) Corrected subcells

Figure : 6th-order corrected DG on a 576 cells mesh after one period

Linear advection equation of a crenel signal $\boldsymbol{A} = (1, 1)^t$

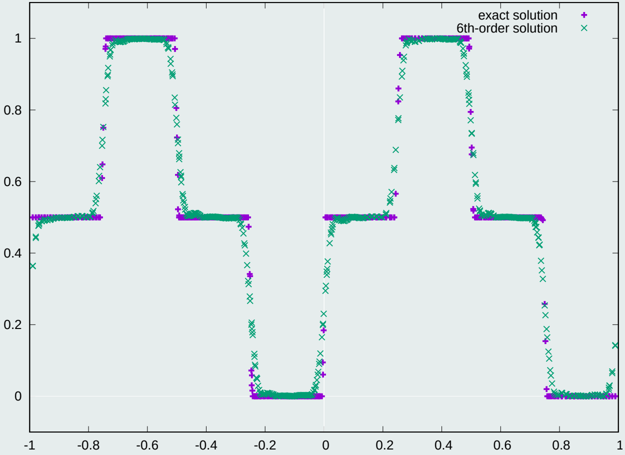

Figure : 6th-order corrected DG on a 576 cells mesh after one period: solution profiles along $x = y$

2D solid body rotation

- $\partial_t u(\boldsymbol{x},t) + \boldsymbol{A}(\boldsymbol{x}) \,.\, \nabla_x u(\boldsymbol{x},t) = 0$ with $\boldsymbol{A}(\boldsymbol{x}) = (0.5 - y,\, x - 0.5)^t$
- $u(\boldsymbol{x},0) = u_0(\boldsymbol{x})$

Rotation of a composite signal: 4th-order intial solutions

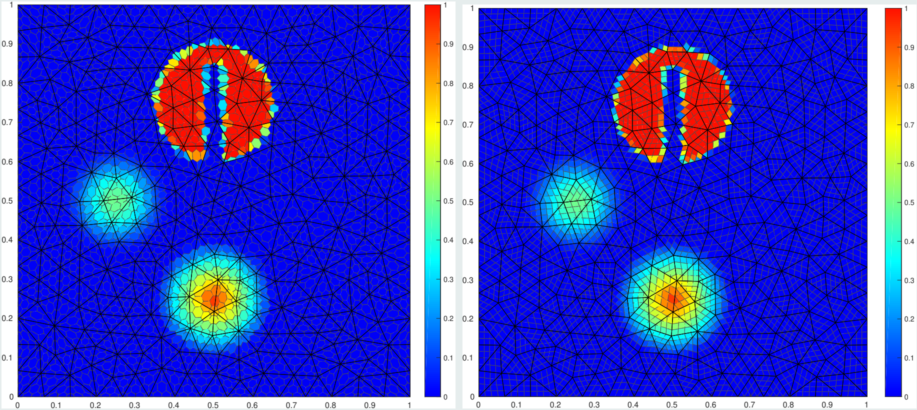

(a) Polygonal subdivision (b) Cartesian subdivision

Rotation of a composite signal after 5 periods

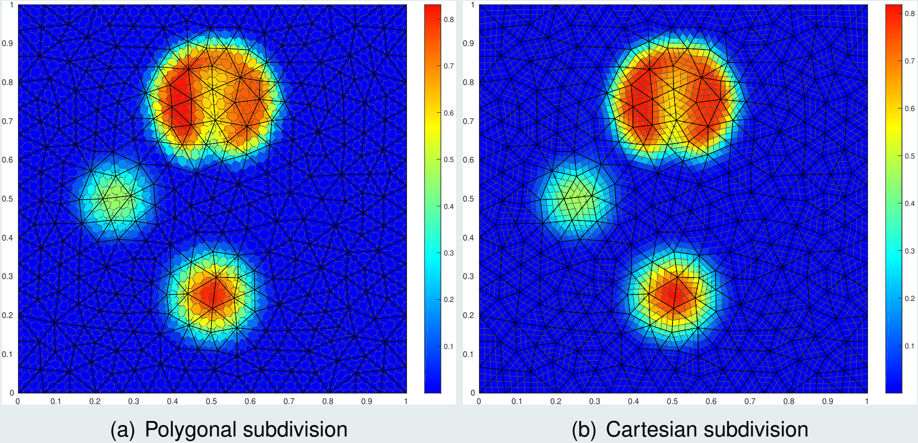

Figure : 4th-order corrected DG on a 576 cells mesh after 5 periods

Rotation of a composite signal after 5 periods

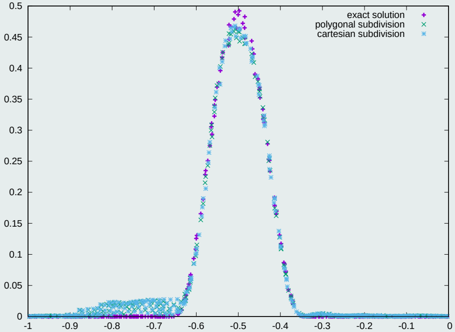

(a) $x = 0.25$

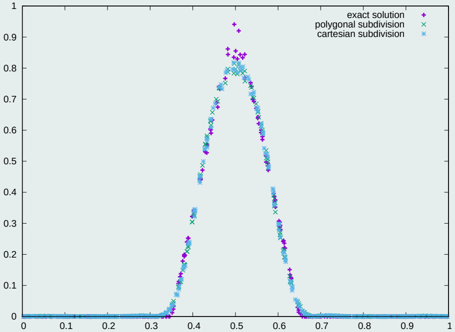

(b) $y = 0.25$

Figure : 4th-order corrected DG on a 576 cells mesh after 5 periods: solution profiles

Rotation of a composite signal after 5 periods

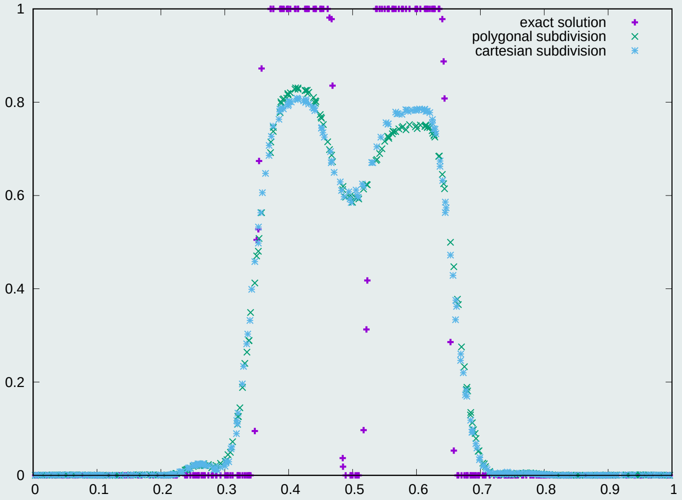

Figure : 4th-order corrected DG on a 576 cells mesh after 5 periods: solution profiles for $y = 0.75$

Rotation of a composite signal after 1 period

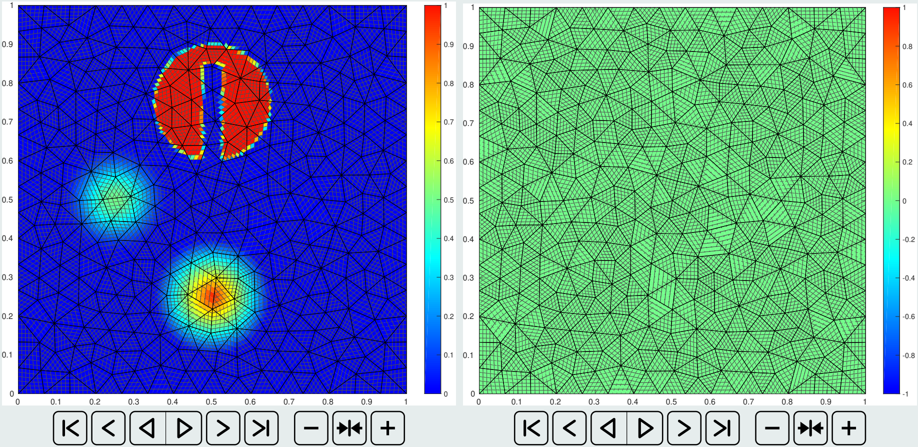

(a) Solution map (b) Corrected subcells

Figure : 6th-order corrected DG on a 576 cells mesh after 1 period

Rotation of a composite signal after 1 period

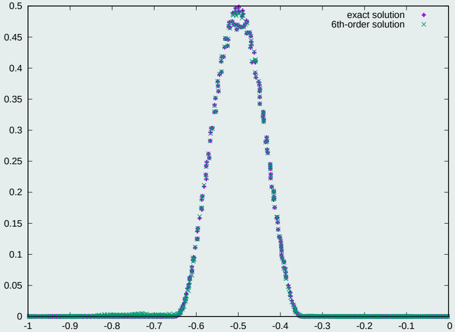

(a) $x = 0.25$

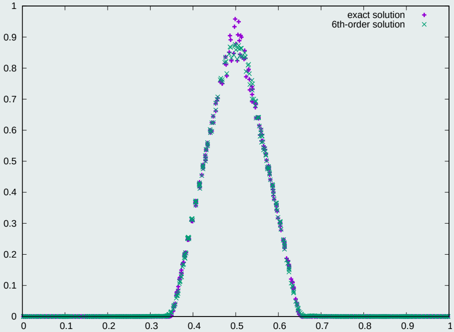

(b) $y = 0.25$

Figure : 6th-order corrected DG on a 576 cells mesh after 1 period: solution profiles

Rotation of a composite signal after 1 period

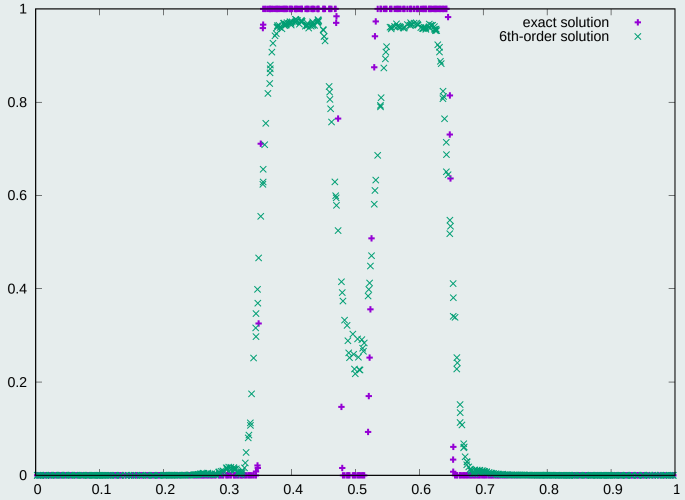

Figure : 6th-order corrected DG on a 576 cells mesh after 1 period: solution profiles for $y = 0.75$

NAD: neighboring subcells set **non-linear problems**

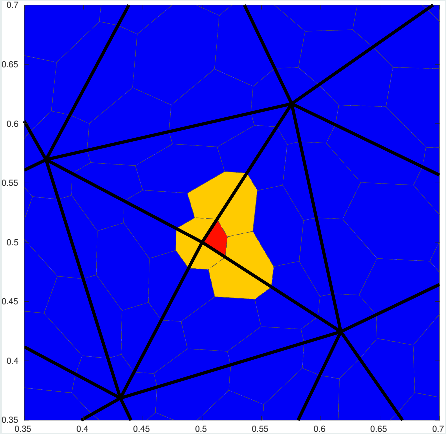

(a) 4th-order, polygonal subdivision

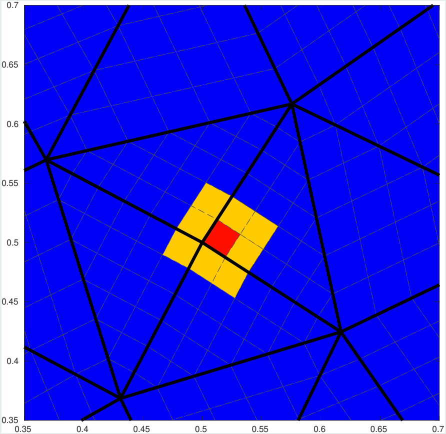

(b) 6th-order, structured subdivision

Figure : Neighboring subcells set for the numerical admissibility criterion

2D non-linear Burgers equation

- $\partial_t u(\boldsymbol{x},t) + \nabla_x \cdot \boldsymbol{F}(u(\boldsymbol{x},t)) = \boldsymbol{0}$ with $\boldsymbol{F}(u) = \frac{1}{2}\left(u^2,\, u^2\right)^{t}$
- $u(\boldsymbol{x},0) = u_0(\boldsymbol{x})$

Burgers equation with $u_0(x,y) = \sin(2\pi\,(x+y))$

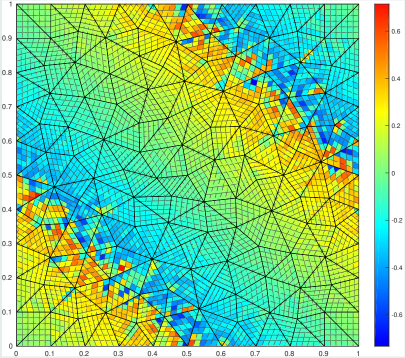

(a) Solution map

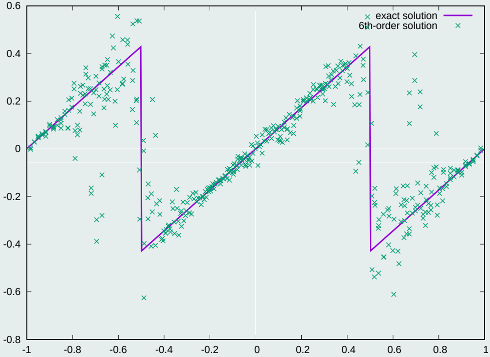

(b) Solution profile

Figure : 6th-order uncorrected DG on a 242 cells mesh at $t = 0.5$

Burgers equation with $u_0(x, y) = \sin(2\pi\,(x + y))$

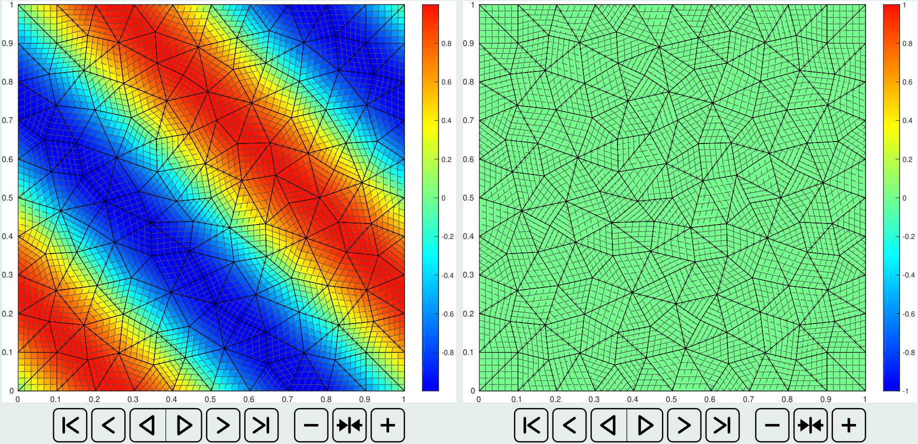

(a) Solution map (b) Corrected subcells

Figure : 6th-order corrected DG on a 242 cells mesh at $t = 0.5$

Burgers equation with $u_0(x, y) = \sin(2\pi\,(x + y))$

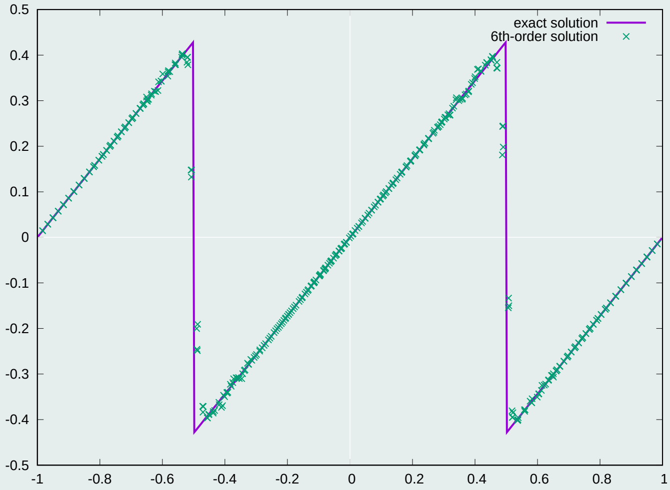

Figure : 6th-order uncorrected DG on a 242 cells mesh at $t = 0.5$: solution profile

Burgers equation with $u_0(x, y) = \sin(2\pi\,(x + y))$

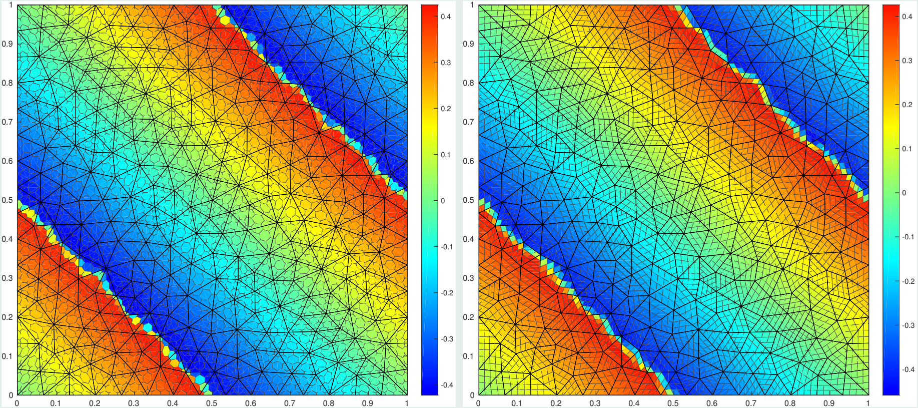

(a) Polygonal subdivision

(b) Cartesian subdivision

Figure : 4th-order corrected DG on a 576 cells mesh at $t = 0.5$: solution profiles

Burgers equation with $u_0(x, y) = \sin(2\pi\,(x + y))$

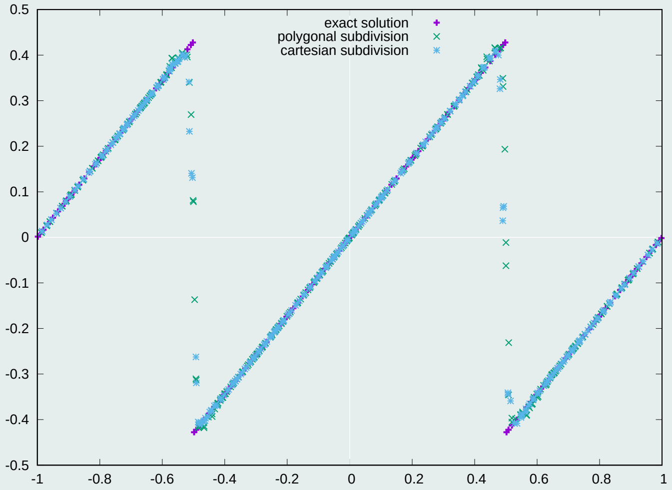

Figure : 4th-order corrected DG on a 576 cells mesh at $t = 0.5$: solution profiles

2D Kurganov, Petrova, Popov (KPP) non-convex flux equation

- $\partial_t u(\boldsymbol{x},t) + \nabla_x \cdot \boldsymbol{F}(u(\boldsymbol{x},t)) = \boldsymbol{0}$ with $\boldsymbol{F}(u) = (\sin u, \cos u)^t$
- $u(\boldsymbol{x},0) = u_0(\boldsymbol{x})$

KPP non-convex flux problem

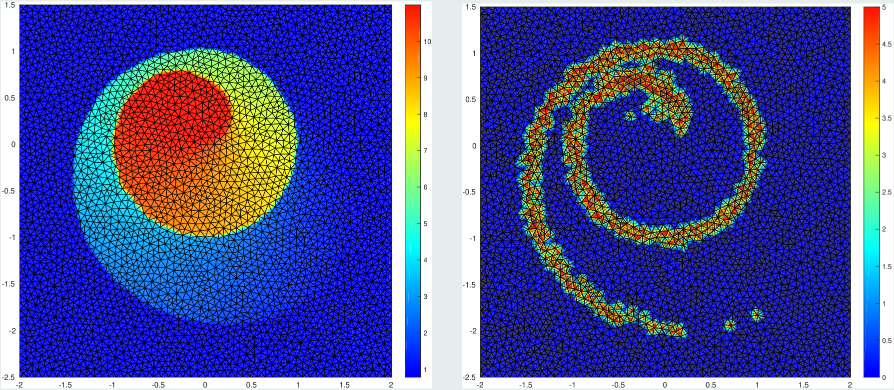

(a) Solution map

(b) Corrected subcells

Figure : 3rd-order corrected DG solution on a 6670 cells mesh

KPP non-convex flux problem

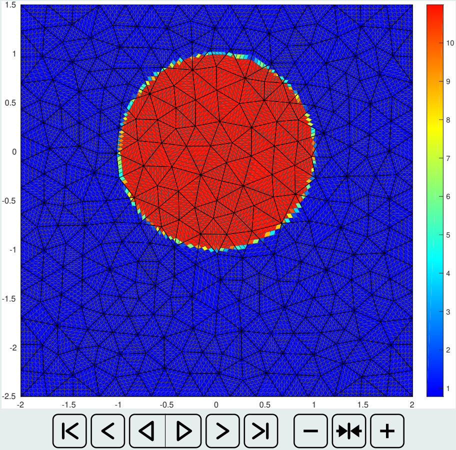

(a) Solution map

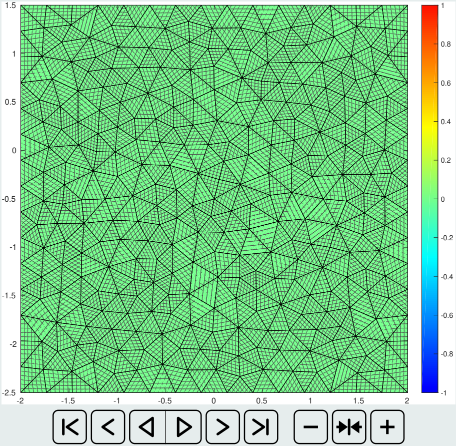

(b) Corrected subcells

Figure : 6th-order corrected DG solution on a 576 cells mesh

2D non-linear Euler compressible gas dynamics equations

- $\partial_t \boldsymbol{V} + \nabla_x \boldsymbol{.}\, \boldsymbol{F}(\boldsymbol{V}) = \boldsymbol{0}$
- $\boldsymbol{V} = \begin{pmatrix} \rho \\ \boldsymbol{q} \\ E \end{pmatrix}$ <u>conservative variables</u>
- $\boldsymbol{F}(\boldsymbol{V}) = \begin{pmatrix} \boldsymbol{q} \\ \dfrac{\boldsymbol{q} \otimes \boldsymbol{q}}{\rho} + p \\ (E + p)\,\dfrac{\boldsymbol{q}}{\rho} \end{pmatrix}$ <u>flux function</u>
- $p := p(\boldsymbol{V}) = (\gamma - 1)\left(E - \dfrac{1}{2}\,\dfrac{\|\boldsymbol{q}\|^2}{\rho}\right)$ <u>equation of state</u>

Sod shock tube problem in cylindrical geometry

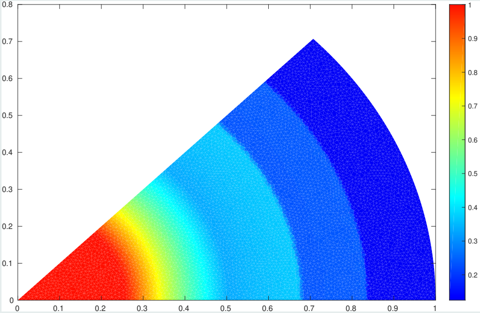

(a) Density map

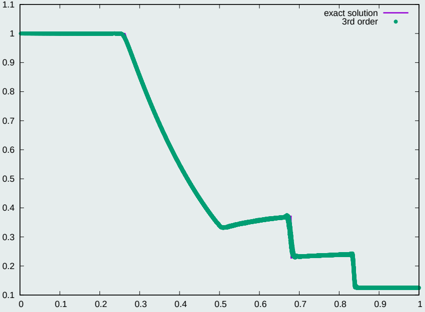

(b) Density profile

Figure : 3rd-order corrected DG on a 10571 cells mesh at $t = 0.2$

Sod shock tube problem in cylindrical geometry

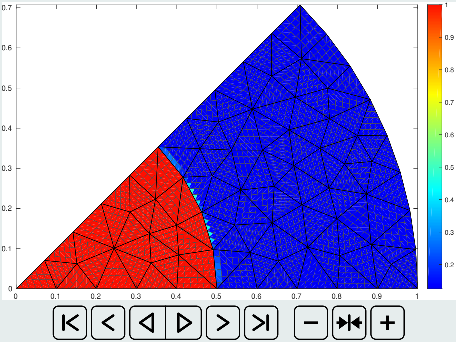

(a) Density map

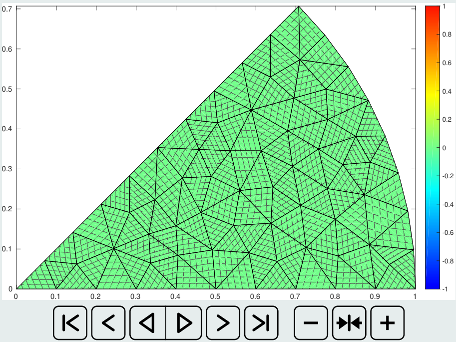

(b) Corrected subcells

Figure : 6th-order corrected DG solution on a 110 cells mesh

Sod shock tube problem in cylindrical geometry

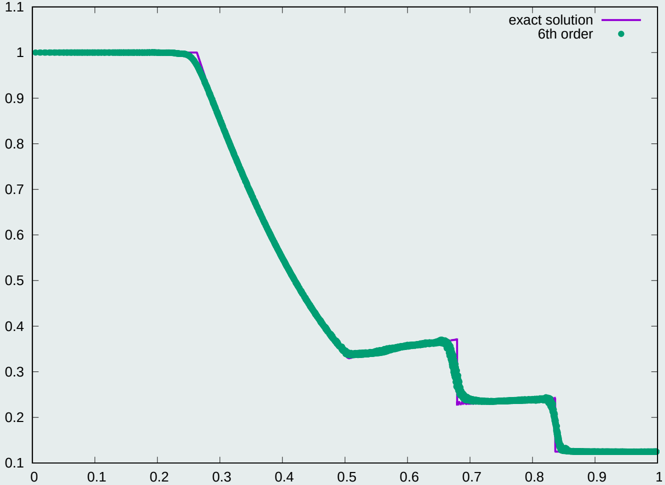

Figure : 6th-order corrected DG solution on a 110 cells mesh

Sedov point blast problem in cylindrical geometry

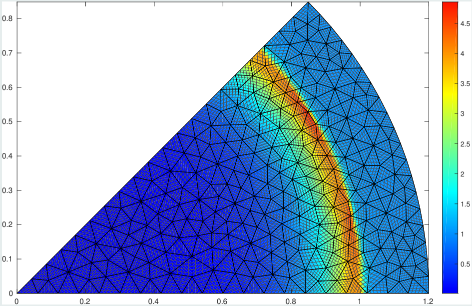

(a) Density map

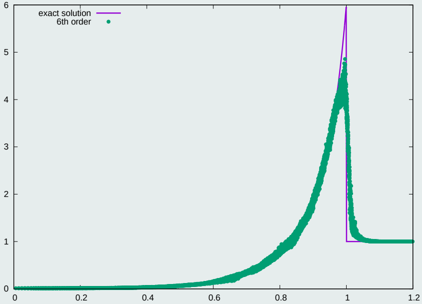

(b) Density profile

Figure : 6th-order corrected DG on a 477 cells mesh at $t = 1$

A Mach 3 wind tunnel with a step

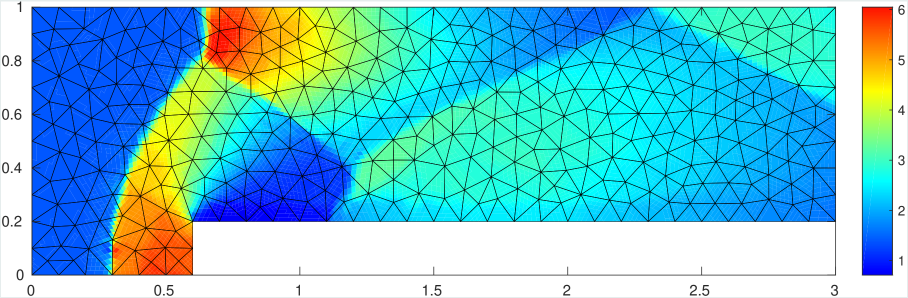

Figure : 6th-order corrected DG on a 680 cells mesh at $t = 4$: density map

Ongoing work

- *A posteriori* FV local subcell correction of high-order DG schemes for the 1D shallow-water equations (**Ali Haidar, Fabien Marche**)
- Extension to the context of ALE Shallow Water sytem of equations coupled with a moving object (**Ali Haidar, Fabien Marche**)
- DoF based adaptive DG scheme through subcell Finite Volume formulation (**Raphaël Loubère**)

Future work

- Maximum principle DG scheme through subcell reconstructed FCT
- Application to 2D Lagrangian hydrodynamics on curvilinear grids
- Extension to 2D Shallow Water-sytem of equations on unstructured grids (**Ali Haidar**)

Articles on this topic

F. Vilar and R. Abgrall, *A posteriori local subcell correction of DG schemes through Finite Volume reformulation on unstructured grids.* **Article in preparation**.

A. Haidar, F. Marche and F. Vilar, *A posteriori Finite-Volume local subcell correction of high-order discontinuous Galerkin schemes for the non-linear shallow-water equations*. JCP, 2021. **Article under revision**.

F. Vilar, *A Posteriori Correction of High-Order DG Scheme through Subcell Finite Volume Formulation and Flux Reconstruction.* JCP, 387:245-279, 2018.